A STUDY ON THE MECHANICAL INTERACTION BETWEEN SOIL AND COLLOIDAL SILICA GEL FOR GROUND IMPROVEMENT

C. WONG, M. PEDROTTI, G. EL MOUNTASSIR & R.J. LUNN

ABSTRACT

In this paper, we explore the mechanical performance of colloidal silica grout to assess its potential for ground stabilisation and hydraulic barrier formation during decommissioning of major industrially contaminated sites. We consider two colloidal silica -soil systems: sand grouted with colloidal silica and kaolin clay mixed with colloidal silica. The aims of the paper are to evaluate the drained stress-strain behaviour (1-D compression and shear resistance) of colloidal silica-soil systems and to determine the particle interactions between soil and colloidal silica at a micron-scale so as to provide an understanding of the macroscopic mechanical behaviour. Two different colloidal silica-soil interaction mechanisms have been found: formation of a solid, cohesive matrix for the case of grouted sand, and increase of the clustering of clay particles for the case of clay mixtures. This paper illustrates for the first time that even under drained conditions colloidal silica can provide mechanical improvement. Colloidal silica-grouted sand showed an increased stiffness and enhanced peak friction angle, while still having a very low hydraulic conductivity (~10^{-10} m/s), typical of intact clay. Similarly, clay-colloidal silica mixtures showed reduced volumetric deformation, increased stiffness for low values of stress (~100kPa), and increases in both the peak and the ultimate shear strength. Our results show that colloidal silica could be deployed in environments where not only hydraulic containment is critical, but where reduced deformation and enhanced resistance to shearing would be beneficial, for example in landfill capping or in the outer fill

layers of embankments designed to minimise internal seepage and infiltration.

1. INTRODUCTION

Over the last thirty years, Colloidal Silica (CS) has been investigated, and more recently deployed, as a low viscosity grout for permeation grouting in soils and for grouting fractured rock. CS has a number of properties that make it attractive. It has an initially low viscosity (close to water) which means that very low injection pressures are required (Moridis et al., 1995). The gel time of CS can be controlled from minutes to several days (Iler, 1979, Yates, 1990) and, once gelled, it has a hydraulic conductivity in the order of 10^{-9} m/s (Moridis et al., 1996a). In addition, it is considered to be environmentally inert (Moridis et al., 1995) and with particle sizes <100nm, it has high penetrability (Iler, 1979, Yates, 1990, Persoff et al., 1995, Moridis et al., 1995).

The key material property that makes CS attractive for use in ground engineering is undoubtedly its low hydraulic conductivity. As such it has been investigated for (i) controlling fluid flow around wellbores within the petroleum industry (Jurinak and Summers, 1991), (ii) as a permeation grout for barrier systems for contaminated sites (Persoff et al., 1995, Moridis et al., 1995, Moridis et al., 1996a, Moridis et al., 1996b, Hakem et al., 1997, Moridis et al., 1999, Persoff et al., 1999, Manchester et al., 2001), and (iii) for preventing water ingress in the tunnelling and underground construction industry (Bahadur et al. (2007), Butrón et al. (2010).

However, CS also provides some level of mechanical improvement. Indeed, a field test by (Moridis et al., 1995) showed that "CS imparted sufficient structural strength to the matrix to permit 10ft high vertical sections of the matrix (characterized by very loose, friable, and heterogeneous materials) to stand without collapsing". CS has also been investigated as a means of increasing resistance to liquefaction in loose sands (Gallagher and Mitchell, 2002, Gallagher and Finsterle, 2004, Gallagher et al., 2007, Gallagher and Lin, 2009, Huang and Wang, 2016), and as stabilizer for collapsible clayey soils (Iranpour, 2016).

Despite its consideration for use in a range of different applications, limited data exist which characterise the mechanical behaviour of grouted soils. The behaviour of pure CS silica has been investigated (Axelsson, 2006, Funehag and Fransson, 2006, Funehag and Gustafson, 2008, Butrón et al., 2009) indicating the fragile nature of the gel. To date the mechanical behaviour of grouted soils which has been reported has been largely limited to the undrained behaviour of grouted sand. Unconfined compressive strength (UCS) tests of grouted soil samples have been reported which demonstrate that grouted-sand specimens have UCS values up to several hundreds of kPas and that increasing the concentration of silica in the colloidal suspension increases the UCS and that UCS increases with curing time (Persoff et al., 1999, Gallagher and Mitchell, 2002, Liao et al., 2003, Mollamahmutoglu and Yilmaz, 2010, Changizi and Haddad, 2017). Undrained triaxial tests have also been conducted which demonstrate the reduced deformation of grouted sand specimens (and hence reduced loss of strength) when subjected to cyclic loading (to simulate earthquake loading) as a means of assessing its potential to mitigate against liquefaction (Gallagher and Mitchell, 2002). A reduction in compressibility and reduced strain at failure has also been observed for clayey soil when mixed with a small amount of colloidal silica (less than 1% by weight) (Changizi and Haddad, 2017).

The small increase in the mechanical resistance (an increase in the cohesion and a decrease in the compressibility) coupled with the well-documented large reduction in hydraulic conductivity (and hence increase in consolidation time) makes CS grouting or CS soil mixtures a promising technique for a range of soil stabilization applications. In particular, the undrained results reported to date in the literature indicate its potential for short-term stability problems e.g. for temporary excavations, cuttings immediately after excavation, tunnelling and construction in earthquake prone areas. In this paper, we explore the drained behaviour of CS-soil systems to assess its potential for use in other ground improvement applications. The drained behaviour of CS-soil systems has not been investigated until now.

In this research we consider two CS-soil systems: sand grouted with CS and kaolin clay mixed with CS. The former is to simulate soil grouted via permeation grouting and the latter to investigate a potential new material for ground engineering. The aims of the paper are (1) to evaluate the drained stress-strain behaviour (1-D compression and shear resistance) of CS-soil systems and (2) to determine the particle interactions between soil and colloidal silica at a micron-scale so as to provide an understanding of the macroscopic mechanical behaviour.

2. MATERIALS AND SPECIMEN PREPARATION

Five different materials were used during this experimental campaign: CS gel only, Leighton Buzzard sand only, Leighton Buzzard sand grouted with CS, kaolin clay only and kaolin clay mixed with CS. The preparation methods for these materials are each described in-turn.

2.1 CS gel

Colloidal silica is an aqueous dispersion of silica particles (Figure 1), which are generally uniform in size and can range from several, to hundreds, of nanometres. A colloidal silica dispersion can be destabilized (Figure 1b) via the controlled application of an electrolyte. Once destabilized, silica particles form siloxane bonds (Si-O-Si), resulting in an increase in the viscosity (Figure 1a and Figure 1c) and eventually a connected matrix of nano-particles, i.e. a gel (Figure 1b). The gelation rate and the gel time (Figure 1b) can be controlled by varying several factors including: particle size, particle concentration, pH, electrolyte concentration, valency and temperature (Iler, 1979, Pedrotti et al., 2017). Hence, colloidal silica grouting requires the combination of two components: the colloidal silica suspension itself and the addition of an electrolyte. In this study Meyco MP320 colloidal silica was used. MP320 has a 40% silica weight concentration, a nominal particle size of 15 nm and a density of 1300 kg/m^3. The specific gravity of the silica particles is estimated to be 2.11.

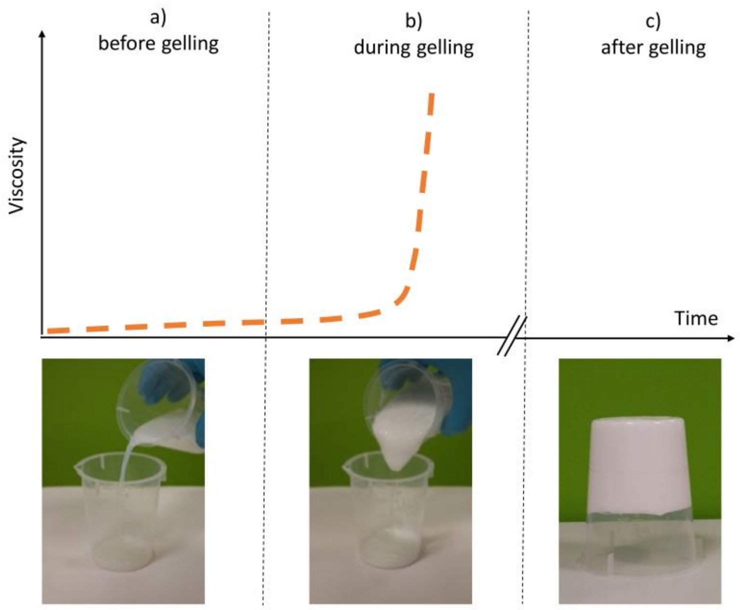

Figure 1. Gelling of CS: a) CS before gelling, b) CS close to the gel time, c) CS after gelling.

To prepare the CS gel samples, CS and the electrolyte solutions were hand mixed in a 5:1 ratio by volume respectively. A solution of NaCl with a concentration of 1.7 M (unless otherwise specified), giving a final electrolyte concentration in the grout mix of 0.28 M, was used in order to obtain a 1 hour gel time. The corresponding rapid increasing in viscosity ended and a firm gel was obtained within a period of approximately less than two hours. The required electrolyte concentrations were determined using the analytical model described in Pedrotti et al. (2017).

In order to reduce water evaporation during sample preparation, once the CS and the electrolyte solution were mixed, all specimens were placed in a chamber and kept at 20°C and 90% relative humidity (90% RH) until gelled. Once gelled, the specimens were cured. Unless otherwise specified, all samples were cured for 1 week by storing under demineralised water at 20°C.

For oedometer testing, specimens of colloidal silica were gelled and cured using the same process, but within the oedometer ring moulds as required for later consolidation testing (Figure 2a). The moulds were made up of a steel oedometer ring with a diameter of 75 mm and thickness of 20 mm attached to a removable plastic base. Silicon grease was applied around the contact between the ring and base to preventing leakage prior to gelling. After curing and subsequent aging, the plastic bases were removed and the oedometer rings containing the CS specimen were placed directly into the oedometer test cell.

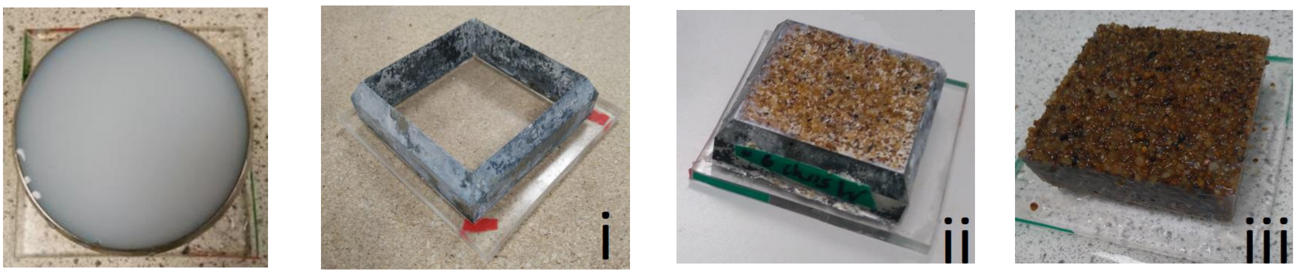

a) b)

Figure 2. Specimen preparation: (a) colloidal silica specimen during curing in oedometer mould, (b) shearbox specimen *i*. mould, *ii*. sand grouted with CS in mould and *iii*. grouted sand specimen after curing and removal from mould.

2.2 Leighton Buzzard sand/ Leighton Buzzard sand grouted with CS

Leighton Buzzard sand with a d_{50} of 1.2 mm, a specific gravity of 2.65 and a coefficient of uniformity of 1.26 was used for all tests. Sand was washed prior to the experiment in order to remove any fines.

For oedometer testing, the oedometer cutting ring was filled with sand, and a plastic syringe was used to measure the required volume of CS. The grouting process was carried out simply by pouring the CS on top of the sand (i.e. the syringe was not embedded). The oedometer cutting ring was attached to a removable plastic base, the edges were sealed with silicon grease to prevent grout leakage prior to the gel time. 148g of Leighton Buzzard sand were grouted with 39 ml of CS mixture.

Specimens were subsequently gelled and cured, as described for the CS samples. For CS grouted sand, each sample was prepared using a NaCl solution resulting in a gel time of approximately 1 hour.

Sand and CS grouted sands were also tested in a shear box. For the shear box, each specimen was prepared by placing 124 g of dry sand into a mould 60 mm x 60 mm x 20 mm height (Figure 2b-i and Figure 2b-ii.). Each specimen was then saturated with 28 ml colloidal silica grout prepared using NaCl. Each square mould had a plastic base, with silicon grease applied at the contact between the mould and base. After curing and subsequent aging, the plastic mould bases were simply detached and, using an extraction tool, the grouted soil specimens (Figure 2b-iii) were transferred into the shear box without damage.

2.3 Kaolin clay/ Kaolin clay mixed with CS

Speswhite kaolin with a plastic limit (w_P) of 0.32 and a liquid limit (w_L) of 0.64 was used for the tests presented in this paper. The grain size distribution shows it is composed of 20% silt-sized particles and 80% clay-sized particles. Kaolin clay specimens were prepared reconstituted from slurry with a water content equal to 1.5w_L (w=0.96).

Specimens of kaolin clay mixed with CS were prepared by hand mixing 100 g of kaolin powder with 153 g of CS to produce a homogeneous slurry (no visible lumps or aggregates). Hand mixing was selected so that results were directly comparable, since it is the standard procedure for preparing clay reconstituted from slurry. This resulted in a specimen made by

100 g of kaolin, 96 g of water and 57g of silica particles. In this way, the ratio between the mass of water (present in the CS) and the mass of solids of kaolin was the same as that for the specimen of kaolin alone ($M_w/M_{s\_kaolin}=0.96$). Using the same concentration of NaCl solution resulted in a slightly shorter gel time in the clay specimens (compared to the sand specimens), this may be a result of less available water in the grout mix (arising from water absorption by clay particles) or due to cation exchange between the clay particles and the grout mix.

For oedometer testing, a pre-mixed specimen (slurry) of kaolin clay and CS was transferred into the oedometer ring mould. The moulds containing the kaolin clay/CS mixture was subsequently left to gel and cure using the process described for the CS specimens.

Speswhite kaolin and CS grouted sands were also tested in a shear box. For the shear box, each specimen was prepared by placing the clay CS mixtures into a mould 60 mm x 60 mm x 20 mm height. As for the oedometer specimens, the moulds containing the kaolin clay/CS mixture was subsequently left to gel and cure using the process described above.

3. EXPERIMENTAL PROCEDURES

3.1 1-D compression tests

1-D mechanical tests were performed in a front-loading oedometer cell (diameter 75 mm) (Controls Testing Equipment Ltd) according to BS 1377-5. All samples were submerged under water in the oedometer cell prior to loading. Samples were compressed in incremental steps to the target vertical stress. Unloading was performed in one single step. For each loading and unloading step, samples were allowed to consolidate for 24h, which was found to be sufficiently long to allow for at least 90% of the consolidation for all samples. For each step, consolidation time (t_{90}) and coefficient of consolidation was calculated according to the conventional Taylor method and subsequently hydraulic conductivity determined. As the initial height and mass of the samples were measured, this was used as a reference point for calculation of the void ratio at each loading step.

3.2 Direct shear tests

Drained direct shearbox tests were conducted using a digital direct shear apparatus (ELE International, Sheffield, UK) according to the BS1377-7 standard (BSI, 1990). For measuring the horizontal shear force and both horizontal and vertical displacements the apparatus is equipped with a 5 kN capacity load cell and two displacement transducers. The internal dimensions of the shearbox body were 60 x 60 mm and 20 mm height. Due to the low hydraulic conductivity of colloidal silica, excess pore water pressure may build up during shearing. From consolidation data, it was determined that a very low shearing rate of 0.001 mm/min was required to prevent pore water pressure build-up and thus maintain drained conditions during shearing. All specimens were sheared at this same rate, with each test therefore taking place over a period of approximately 6 days. Vertical effective stresses of 100, 200, and 300 kPa were applied to reflect stresses in the near subsurface.

Shear tests data performed on kaolin clay reconstituted from slurry and consolidated to 50, 100, 150 and 300 kPa are reported here from Pedrotti (2018) (shear rate 0.02 mm/min) and data for the sample consolidated to 300 kPa from Galvani (2003) (shear rate 0.005 mm/min).

3.3 Suction measurement

The WP4C dew-point potentiometer manufactured by Decagon Device Inc was used to measure total suction for the sample cured at 90% R.H

3.4 Scanning Electron Microscope Imaging

Microscope images were performed by means of a Field Emission Scanning Electron Microscope (Hitachi SU-6600). This apparatus is equipped with energy dispersive spectroscopy, Oxford Inca 350 with 20mm X-Max detector and Wavelength dispersive spectroscopy, Oxford Inca Wave 700 microanalysis system with Energy to allow elemental analysis of metals and ceramic materials.

Microscope images were also obtained using a Tungsten Filament Scanning Electron Microscope (Hitachi S-3700). This apparatus has Energy Dispersive Spectroscopy capability, Oxford Inca 350 with 80mm X-Max detector, to allow elemental analyses of materials.

For SEM imaging specimens were oven dried at 105°C for at least 24hr.

3.5 X-CT imaging

CT images were performed by means of a Nikon XT H 320 XRay CT scanner. No sample preparation is required for x-CT imaging, hence, samples remain entirely undisturbed. In the present work, the voxel resolution was approximately 0.504 mm and the scanner settings were energy 183 kV and current 204 μA.

The reconstruction was carried out using CT Pro and CT Agent software (Nikon-Metrology). The visualisation and analysis of the CT data were performed with AVIZO 9.0.

4. INVESTIGATION ON THE MECHANICAL BEHAVIOUR

The mechanical behaviour of five different materials was investigated in order to highlight the mechanical interaction between soil (i.e. sand and clay) and CS gel. CS gel only, Leighton Buzzard sand only, Leighton Buzzard sand grouted with CS, kaolin clay only and kaolin clay mixed with CS were tested.

4.1 CS gel

1-D compression tests

The mechanical behaviour upon 1-D compression of CS gel was investigated using the oedometer (Figure 3). Figure 3a shows the void ratio change of four CS samples that were cured under demineralised water for 1, 2, 4 and 8 weeks respectively. Since no deformation occurred during curing, the initial void ratio of these samples is the same. The samples cured for 1 and 2 weeks appear to follow a single compression curve. Similarly, the samples cured for 4 and 8 weeks appear to follow a single (but different) compression curve; the 4 and 8 week samples appear to have a stiffer behaviour at low vertical stresses (up to 60 kPa), as if the bonding between silica particles was stronger than the samples cured for less time. As the vertical stress increases the compressibility becomes similar to that of the samples cured for 1 or 2 weeks, although the two pairs of curves never merge. Finally, upon unloading, all four samples exhibit the same small elastic swelling, suggesting that the initial particle bonding (and hence gel structure) was not recovered after yielding.

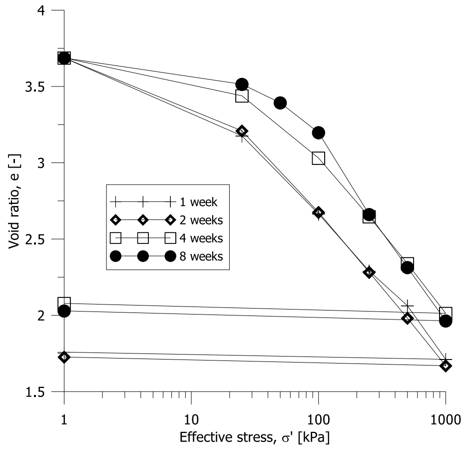

a)

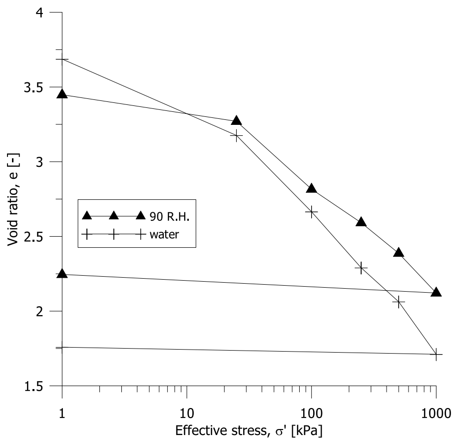

b)

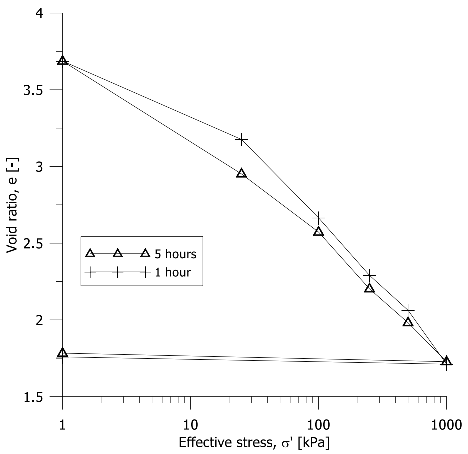

c)

Figure 3. 1-D compression curves for CS samples: a) tested after different curing durations, b) exposed to different evaporation conditions during curing and c) prepared with different gel times.

Figure 3b shows the void ratio change of two CS samples, prepared with a NaCl electrolyte solution and cured for 1 week. One sample (water) was cured under demineralised water (this same sample was reported in Figure 3a and called "1 week") whilst the other was cured at a 90% constant Relative Humidity (90 R.H.). After curing, the two samples were tested in the oedometer cell under saturated conditions. Figure 3b demonstrates that the sample cured at 90% RH has suffered some water loss and undergone shrinkage. Upon saturation in the oeodmeter cell this reduction in volume was not fully recovered and therefore the void ratio at the beginning of the test is smaller than that for the sample cured under water. Upon 1-D compression, the two compression curves diverge and the behaviour of the sample cured at 90% R.H. is stiffer than that of the sample cured under water. In order to investigate the stress conditions at the beginning of consolidation, a similar sample was cured at 90% RH and the total suction was measured. The average suction at the end of curing was measured to be 1620 kPa. Upon drying the lateral earth pressure coefficient is generally unknown, however with a value of suction this high, it seems reasonable to assume that the "equivalent" vertical pre-consolidation stress is higher than 1000 kPa (the maximum vertical stress applied during the oedometer test). Hence, it seems reasonable to ascribe the different compression behaviour between the sample cured in saturated conditions and the sample cured at 90% R.H. to a pre-consolidation stress due to the suction developed in the latter sample. This high suction stress explains the stiffer behaviour of the sample cured at 90% R.H., in terms of over-consolidation (Skempton and Jones, 1944, Sridharan and Nagaraj, 2000). Therefore, no information on whether the normal consolidation compressibility is recovered can be determined, since the pre-consolidation stress was not overwhelmed.

In Figure 3c the effect of the gel time on 1-D compression was investigated. Two samples were prepared by mixing CS with a NaCl electrolyte solution of different concentrations (1.7 M and 1.3 M, such that the samples had gel times of 1 hour and 5 hours respectively. Upon 1-

D compression (after 1 week curing in demineralised water), the difference in the compression curves was well within the repeatability of the test. This result suggests that, within the accuracy of the measurement, there is no difference in the mechanical behaviour due to different rates of electro-chemical bonding between particles in the CS.

The hydraulic conductivity calculated from the 1-D compression test for each sample at every loading step is reported in Figure 4. Values range between 10^{-9} and 10^{-12} m/s. Other than the reduction in hydraulic conductivity with increasing effective vertical stress, there is no clear pattern of behaviour between samples. The high variability of the points at the first steps is probably due to the difficulties to estimate the exact consolidation time because of the long duration of the tests.

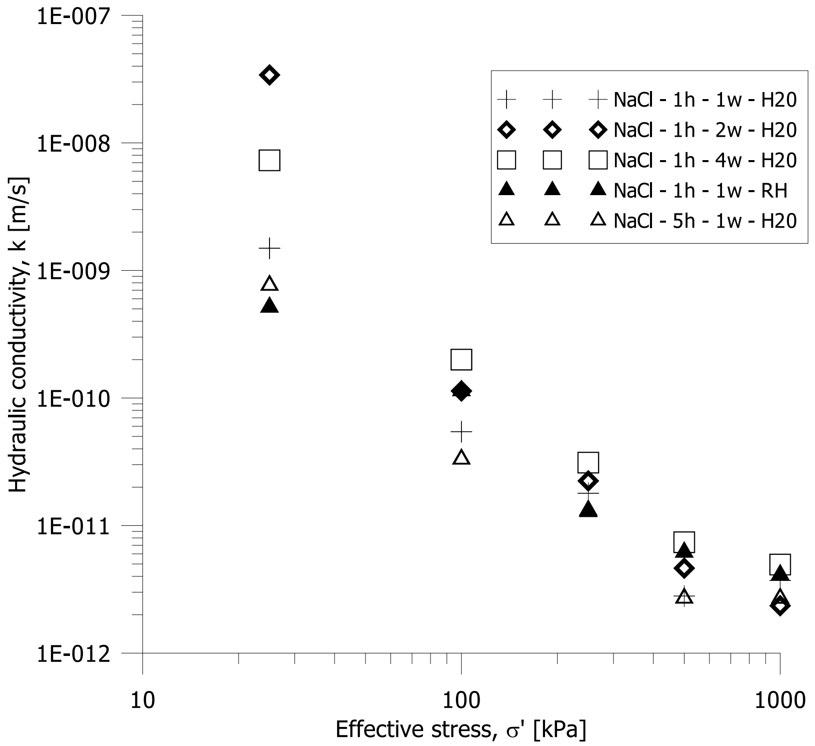

Figure 4 Hydraulic conductivity for different CS samples.

4.2 Sand grouted with CS gel

1-D compression tests and direct shear tests were carried out on Leighton Buzzard sand only and Leighton Buzzard sand grouted with CS.

1-D compression tests

In Figure 5a, the change in void ratio upon 1-D compression of a sample of sand grouted with CS is compared with the change in void ratio of sand only. The two samples were prepared with the same initial density of sand, however the sample of sand grouted with CS shows a void ratio lower than the sample with sand only, this is due to the fact that when calculating the void ratio, the silica nano-particles has been considered as part of the solid fraction.

To overcome this, Figure 5b shows the same test reported in Figure 5a but plots the observed vertical strain against the effective stress. The sample of sand grouted with CS shows a much stiffer response (i.e. reduced volume change) than the sand only sample. For the grouted sand specimen, the compression behaviour remains stiffer than for sand only over the full range of the investigated vertical stress.

It is worth noting that the hydraulic conductivity of sand after CS grouting reduced dramatically. In Figure 5c, the hydraulic conductivity of grouted sand estimated from the consolidation times during the oedometer tests is compared with the hydraulic conductivity of sand only, estimated by using the Hazen's empirical formula (Hazen, 1893) from the grain size analysis. As shown in Figure 5c, the hydraulic conductivity of the CS grouted sand is similar to that expected for a clayey soil (about 10^{-10} *m/s*). Hence to summarise, the CS grouted sand has a high stiffness similar to sandy soils, but a long consolidation time and low hydraulic conductivity, generally characteristic of clayey soils.

(a)

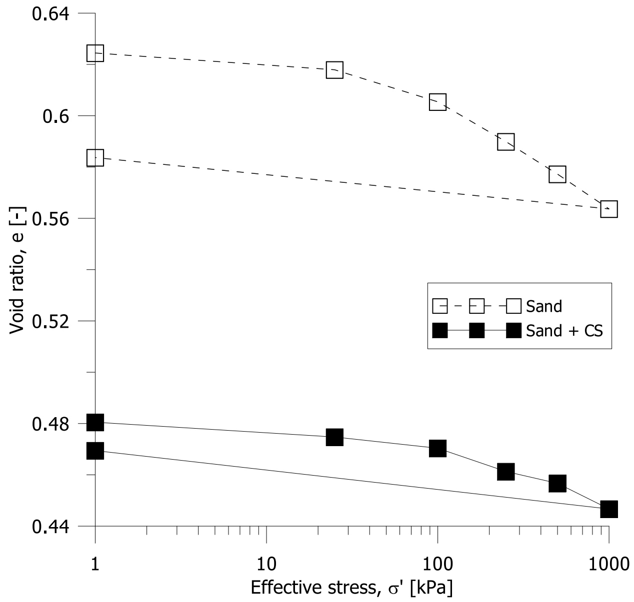
0.64
0.6
0.56
0.52
0.48
0.44
Void ratio, e [-]
1
10
100
1000
Effective stress, σ' [kPa]
Sand
Sand + CS

(b)

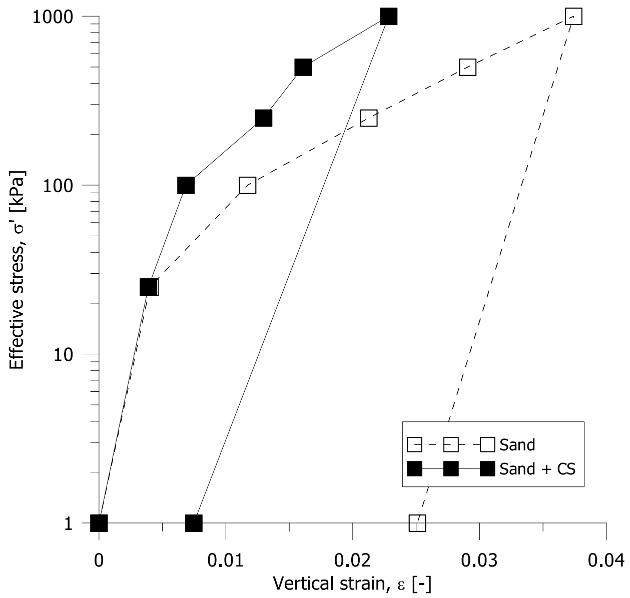
1000
100
10
1
Effective stress, σ' [kPa]
0
0.01
0.02
0.03
0.04
Vertical strain, ε [-]
Sand
Sand + CS

(c)

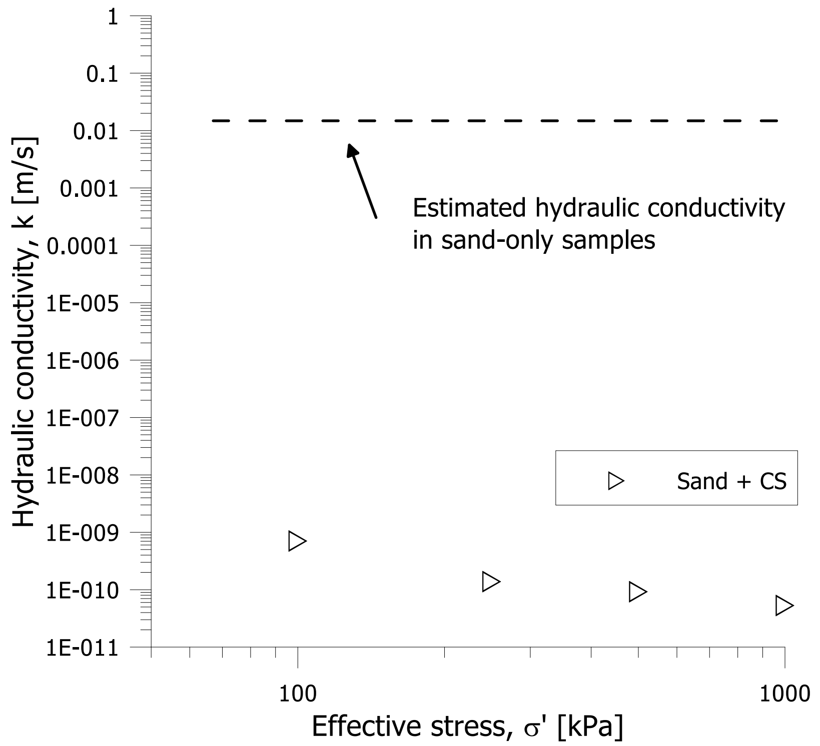

Figure 5. 1-D compression tests of sand and sand grouted with CS: (a) void ratio against effective stress, (b) effective stress against vertical strain and (c) hydraulic conductivity against effective stress

Direct Shear tests

Figure 6 shows the results of a shear test performed on three sand samples, consolidated to 100, 200 and 300 kPa under saturated conditions. In Figure 6a the horizontal displacement versus the shear stress/effective vertical stress ratio ($t/s_v^{'}$) is reported and in Figure 6b the volumetric change in terms of horizontal versus vertical displacement is shown.

At the higher vertical stress (300 kPa) the sand exhibits a compressive behaviour, as the vertical stress decreases (200 and 100 kPa) the volumetric behaviour becomes dilative. As expected, all samples tend toward the same value of ultimate stress, and the sample sheared with the lowest vertical stress has the highest peak stress. In order to take into account the effect of the dilatancy, the ultimate shear stress is here defined according to Taylor (1948).

These are plotted in Figure 6c. For the ultimate conditions the friction angle, $\phi'_{ultimate}$, was computed to be 36 ° and for the peak conditions, the friction angle ϕ'_{peak}=41°. The two envelopes were forced to pass through the origin i.e. no cohesion was allowed.

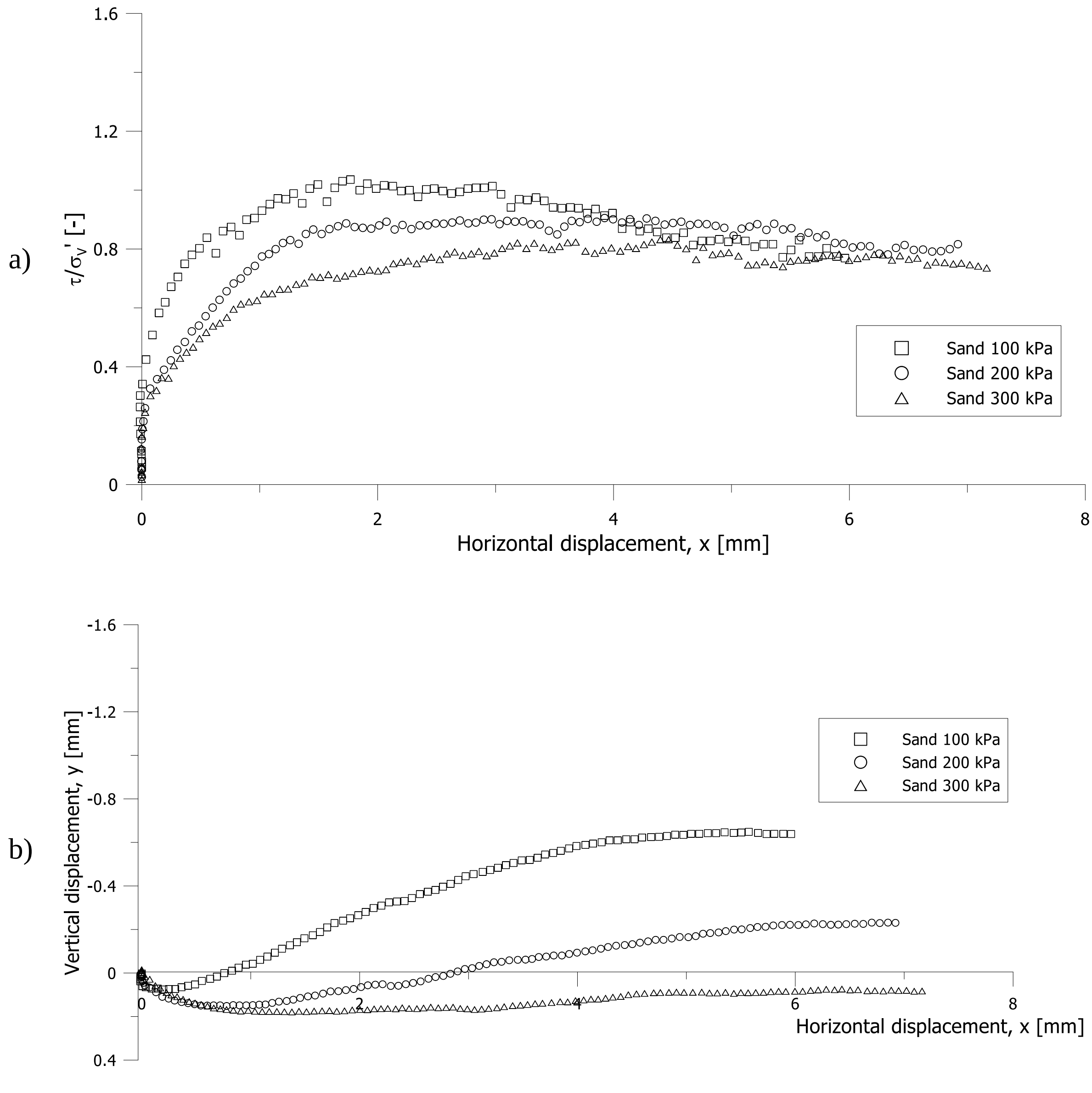

c)

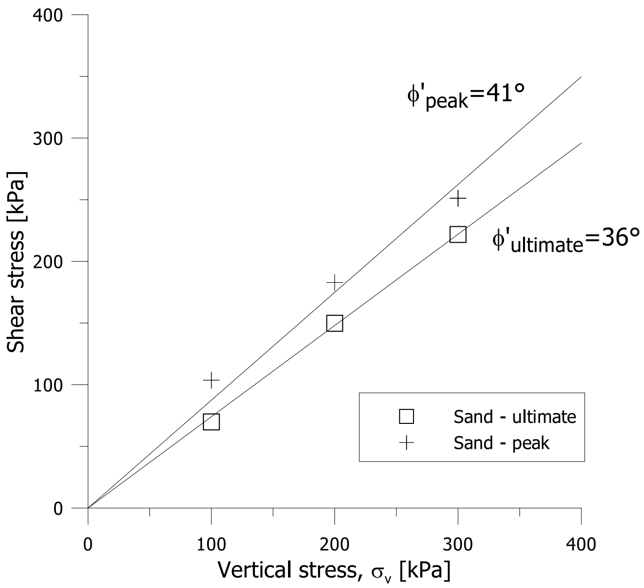

Figure 6. Direct shear test on sand samples at different effective vertical stress. a) horizontal displacement versus the shear stress/effective vertical stress ratio, b) volumetric change and c) Direct shear envelopes for sand samples

Figure 7 (a-f) shows the shear tests performed on samples of sand grouted with CS for the same values of vertical stress (100, 200 and 300 kPa). For each value of vertical stress two samples were prepared, one cured under demineralised water for 1 week and one for 4 weeks. All shear tests were conducted under saturated conditions.

Figure 7a and b show the horizontal displacement versus the t/s'_v and versus the vertical displacement, respectively, for an effective vertical stress of 100 kPa. Test results are plotted for sand only, sand and CS cured for 1 week, sand and CS cured for 4 weeks. Figure 7c, d and Figure 7e, f show the same results for samples sheared under effective vertical stresses of 200 and 300 kPa, respectively.

Looking at Figure 7a, the sample cured for 4 weeks shows an initial stiffer behaviour than the sample cured for 1 week only. This is in agreement with the oedometer tests presented in Figure 3a.

The sand only sample is the least compressible. It appears that the presence of the silica has a lubricating effect (increasing the strain required to reach the peak shear stress) which is counterbalanced by the hardening of the CS for longer curing times.

The two samples grouted with CS exhibit a peak at a similar shear stress/effective vertical ratio, which is about 30% higher than the sample with sand only. After the peak, although the ultimate shear stress of the grouted samples remains slightly higher than the sand–only sample, the three curves appear to be converging. Figure 7b shows that the two grouted samples have a larger dilatancy than the sand-only sample and that the dilatancy increases with increasing curing time.

a)

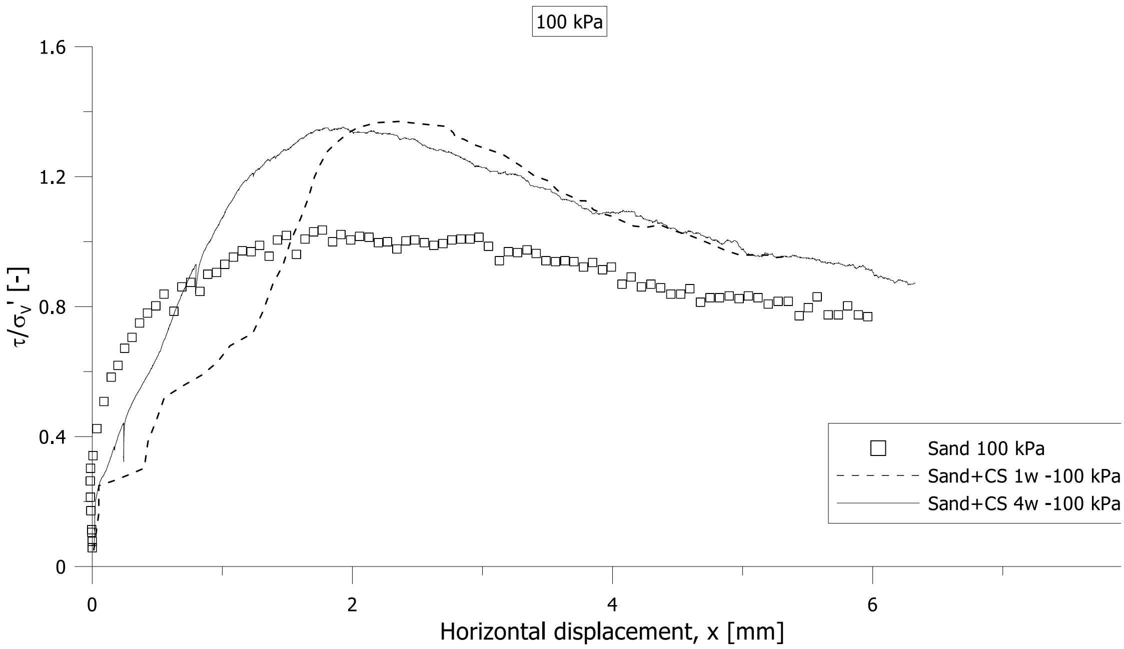

b)

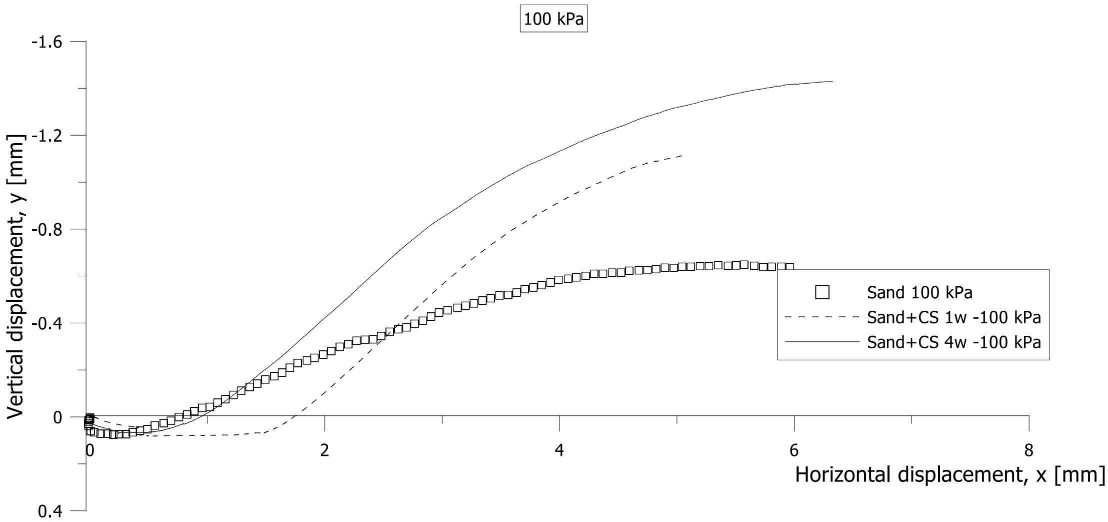
100 kPa
Vertical displacement, y [mm]
Horizontal displacement, x [mm]
-1.6
-1.2
-0.8
-0.4
0
0.4
0
2
4
6
8
Sand 100 kPa
Sand+CS 1w -100 kPa
Sand+CS 4w -100 kPa

c)

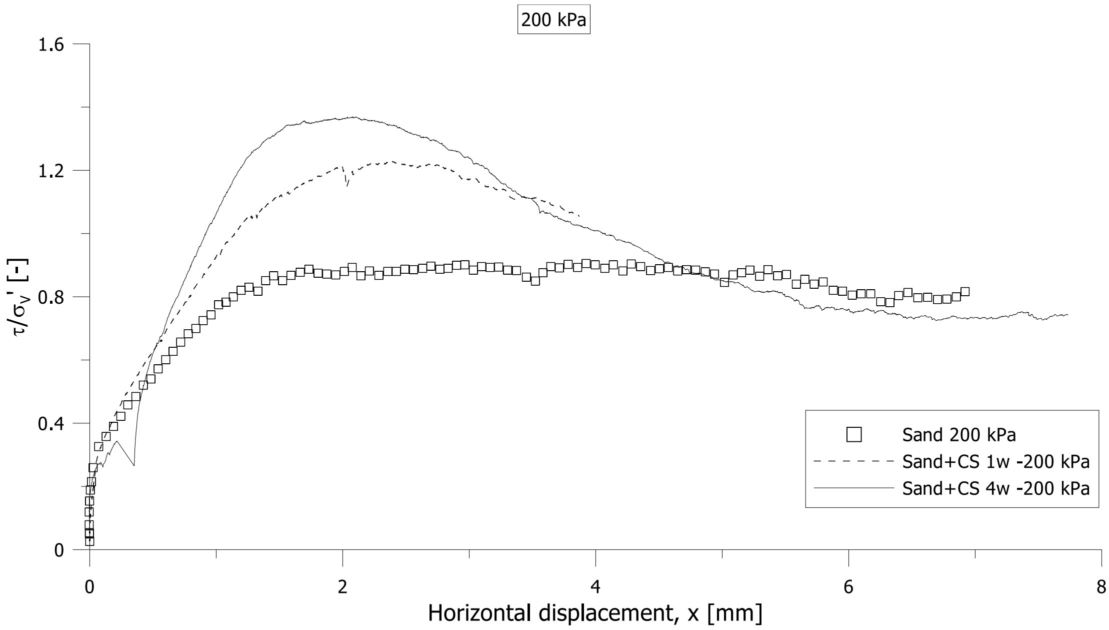
200 kPa
τ/σ_v' [-]
Horizontal displacement, x [mm]
1.6
1.2
0.8
0.4
0
0
2
4
6
8
Sand 200 kPa
Sand+CS 1w -200 kPa
Sand+CS 4w -200 kPa

d)

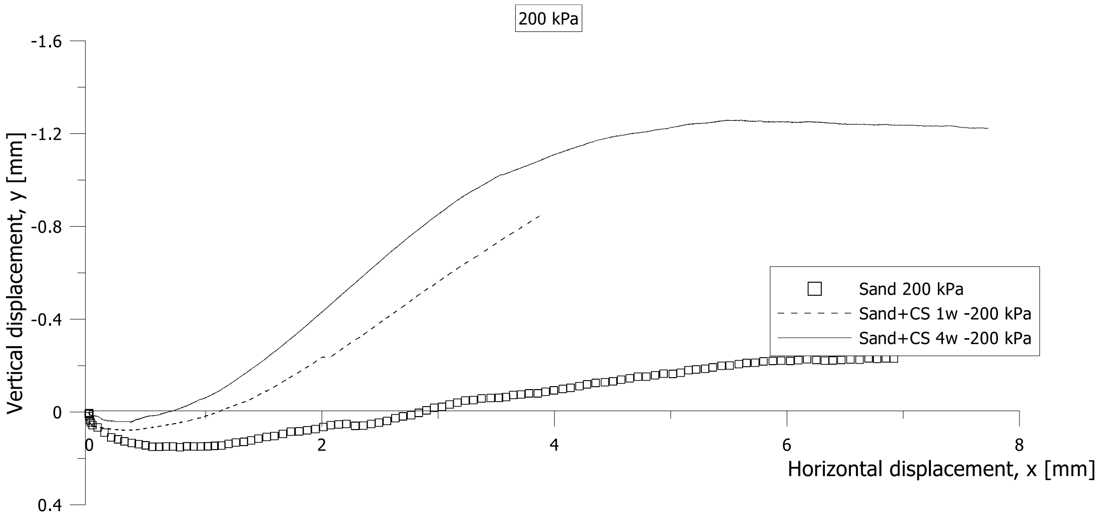
200 kPa
Vertical displacement, y [mm]
Horizontal displacement, x [mm]
Sand 200 kPa
Sand+CS 1w -200 kPa
Sand+CS 4w -200 kPa

e)

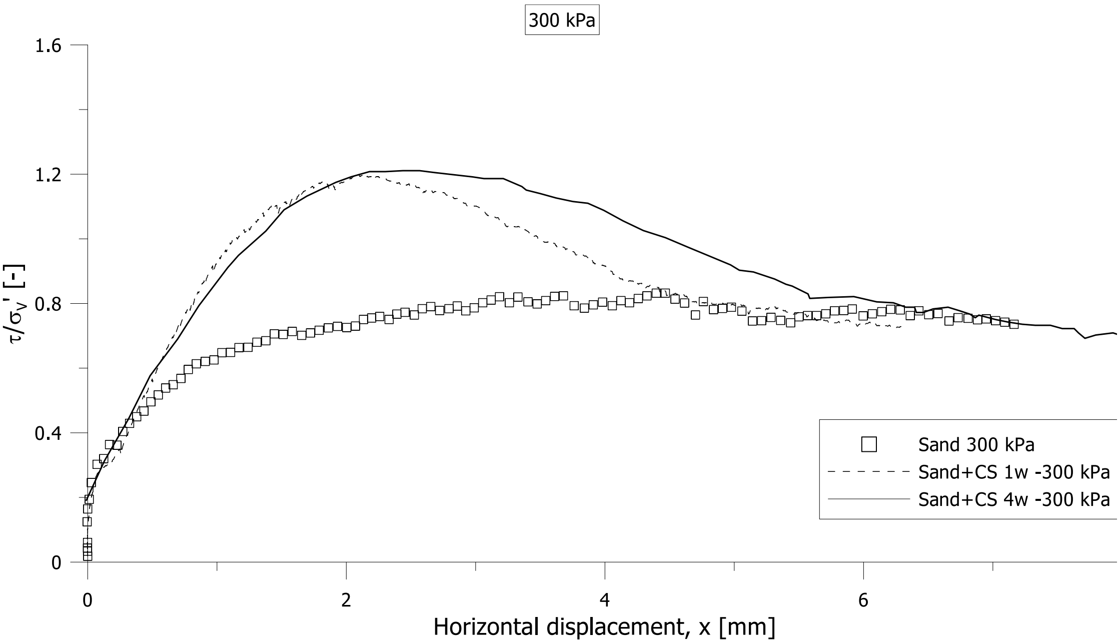
300 kPa
τ/σ_V' [-]
Horizontal displacement, x [mm]
Sand 300 kPa
Sand+CS 1w -300 kPa
Sand+CS 4w -300 kPa

f)

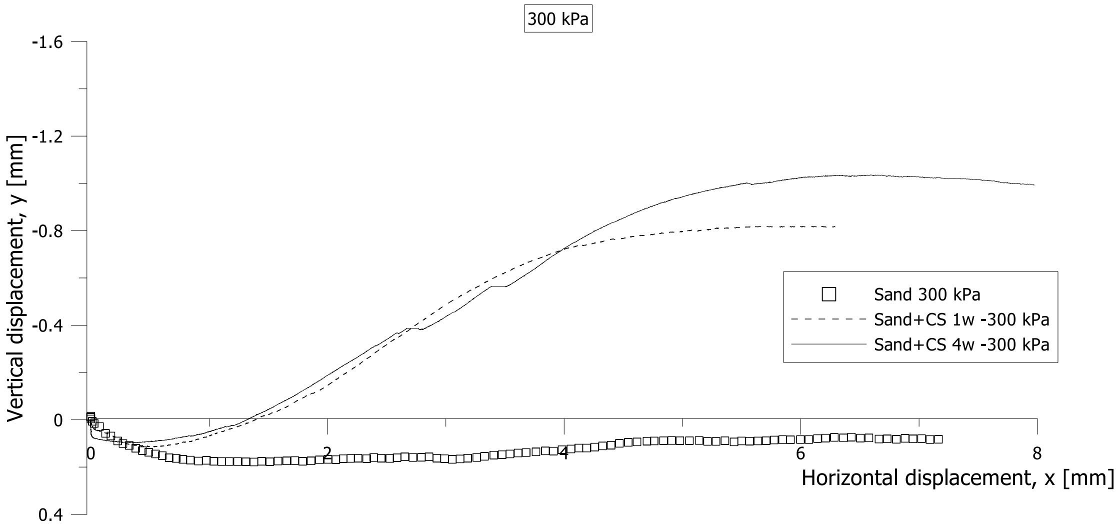

Figure 7. Direct shear test on sand sample grouted with CS. a) horizontal displacement versus the shear stress/vertical stress ratio (effective vertical stress 100 kPa), b) volumetric change (effective vertical stress 100 kPa), c) horizontal displacement versus the shear stress/vertical stress ratio (effective vertical stress 200 kPa), d) volumetric change (effective vertical stress 200 kPa), e) horizontal displacement versus the shear stress/vertical stress ratio (effective vertical stress 300 kPa), f) volumetric change (effective vertical stress 300 kPa).

Analysis of the results at higher vertical stresses in Figure 7c and Figure 7e shows that the general behaviour is very similar to that at 100kPa i.e. all grouted samples show a higher peak stress than with sand-only, and all grouted samples appear to converge to the same ultimate stress as for sand-only. In addition, the volumetric change shown in Figure 7d and Figure 7f is also similar to that in Figure 7b; the grouted samples are dilative and the longer the curing time, the higher the dilatancy.

There are, however, a few differences in behaviour worth noting in the results for the 200kPa and 300kPa samples. In both sets of results, there is no initial difference in stiffness between the grouted samples (regardless of curing time) and the sand only (Figure 7c and

Figure 7e respectively). Hence, the CS lubricating effect appears not to occur at higher vertical stresses and the additional particle bonding given by the CS becomes negligible. Also, for the 200kPa load, (Figure 7c) the grouted sample cured for 4 weeks exhibits a higher peak stress than the sample cured for 1 week, whereas for the 300 kPa load (Figure 7e) the peaks are the same for both curing times.

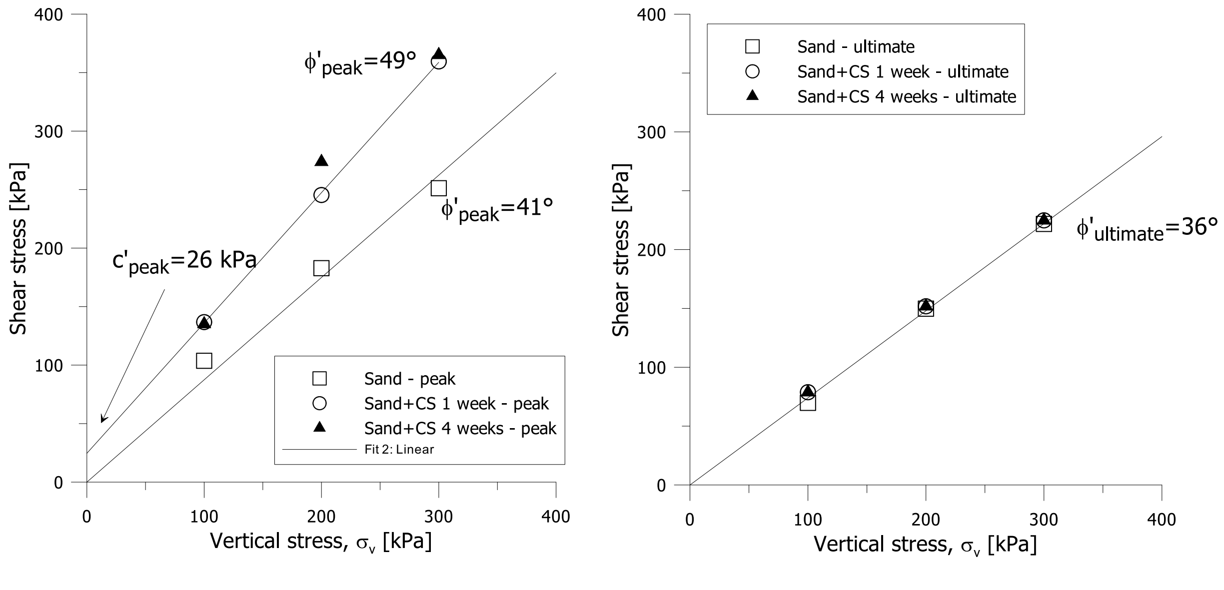

a) b)

Figure 8. Shear envelopes: (a) peak shear stress envelope and (b) ultimate shear stress envelope for sand grouted with CS.

Figure 8a shows the peak shear stress envelope, sand-only specimens have a peak friction angle ϕ'_{peak} of 41° which compares with an average peak friction angle for the grouted samples of 49°. In addition, the grouted samples exhibit a drained cohesion c’ = 26 kPa, which is attributed to bonding provided by the CS matrix before failure. Figure 8b presents the ultimate shear stress envelope for all of the above tests, confirming that they have a friction angle, $\phi'_{ultimate}$, of 36 °. It is worth highlight that the presence of the particle bonding provided by the CS increases the peak shear strength and the drained cohesion at peak conditions.

4.3 Clay mixed with CS

1-D compression tests and direct shear tests were carried out Speswhite kaolin clay mixed with CS. The results were compared with tests on Speswhite kaolin clay only.

1-D compression tests

In Figure 9a, the change in void ratio upon 1-D compression of a sample of kaolin clay mixed with CS is compared with the change in void ratio of a kaolin clay sample reconstituted from slurry. The sample of kaolin clay mixed with CS at the beginning of the compression test had a void ratio smaller than the sample reconstituted from slurry, and was much less compressible for vertical stress lower than 30 kPa. As the vertical stress increases beyond 30kPa, the compressibility of the two samples becomes very similar, although the sample mixed with CS remains denser than the sample reconstituted from the slurry. Despite the similar normal compressibility, the swelling upon unloading was smaller for the sample containing CS than for kaolin only. Hence, it appears that the presence of CS inhibits the recovery of elastic deformation.

In the sample reconstituted from slurry, only kaolin and water are present, whereas in the CS mixed sample, the solid fraction is made up of both kaolin and silica nano-particles. In order to compare the mechanical behaviour, the two samples were prepared with the same Mass of water/Mass of kaolin ratio. As a result the initial void ratio of the two samples is different as the volume of silica particles contributes to the volume of solids present. To overcome this, Figure 9b shows the same test as Figure 9a but plots the observed vertical strain against the effective stress. This clearly shows that the sample prepared by mixing kaolin clay and CS is far less compressible than the sample with kaolin only. The reduced compressibility seems to be related to stiffer behaviour at the lowest load steps, caused by the presence of the CS. Whereas, at higher vertical load, the two samples have the same compressibility.

In Figure 9c the hydraulic conductivity determined during oedometric consolidation of the kaolin and CS mixture is compared with the one of kaolin only. When silica is present the hydraulic conductivity of the sample drops by two orders of magnitude. Indeed, when the kaolin/CS sample is consolidated to 1000 kPa the hydraulic conductivity was determined to be 9.7 x10^{-12} m/s.

a)

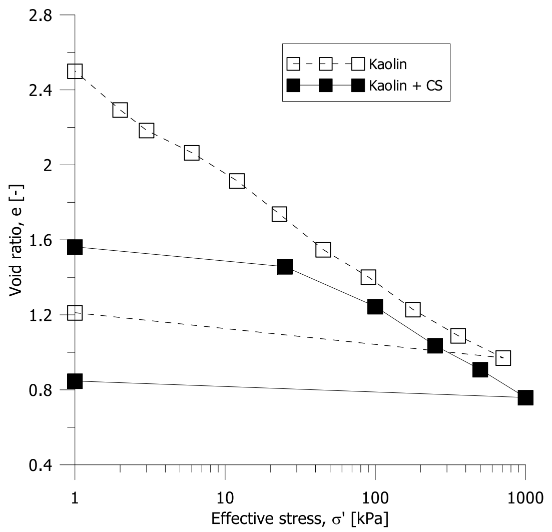

b)

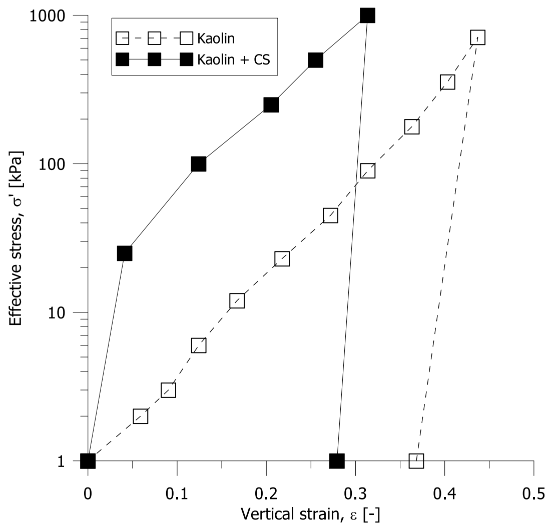

c)

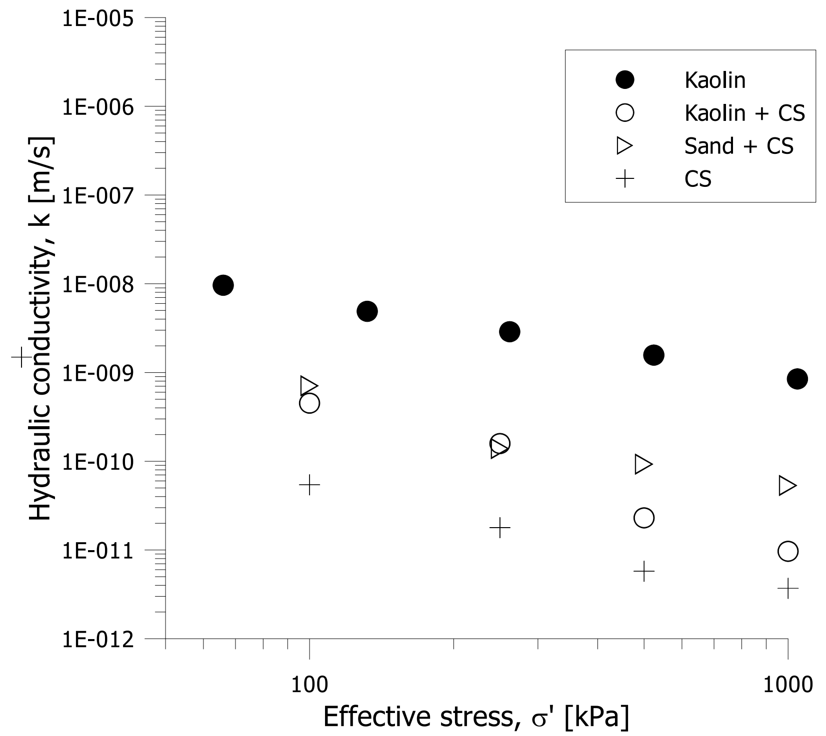

Figure 9. 1-D compression curves for kaolin reconstituted from slurry and kaolin mixed with CS. a) void ratio against effective stress, b) effective stress against vertical strain and (c) hydraulic conductivity upon odeometric compression.

For completeness, also the values of the hydraulic conductivity of the sample of sand grouted with CS (already presented in Figure 5c) is reported and the hydraulic conductivity of CS only (previously reported in Figure 4 as NaCl -1h -1w – H20). It is interesting to note that also the sample of sand grouted with CS shows an hydraulic conductivity one order of magnitude lower than the sample of kaolin clay only and just one order of magnitude higher than CS only.

Direct shear tests

Figure 10 shows the results of a shear test performed on kaolin clay reconstituted from slurry and consolidated to 50, 100, 150 and 300 kPa (data from Pedrotti (2018) and Galvani (2003))

In Figure 10a the horizontal displacement versus the t/s'_{v} is reported and in Figure 10b the volumetric change in terms of horizontal versus vertical displacement is shown. For the four vertical stresses investigated the shear behaviour is similar. All the samples exhibit a compressive behaviour and a very similar ultimate shear stress/effective vertical stress ratio. For the ultimate conditions the friction angle, ϕ'_{ultimate}, was computed to be 16° with a drained cohesion equal to 2 kPa. No peak conditions were considered.

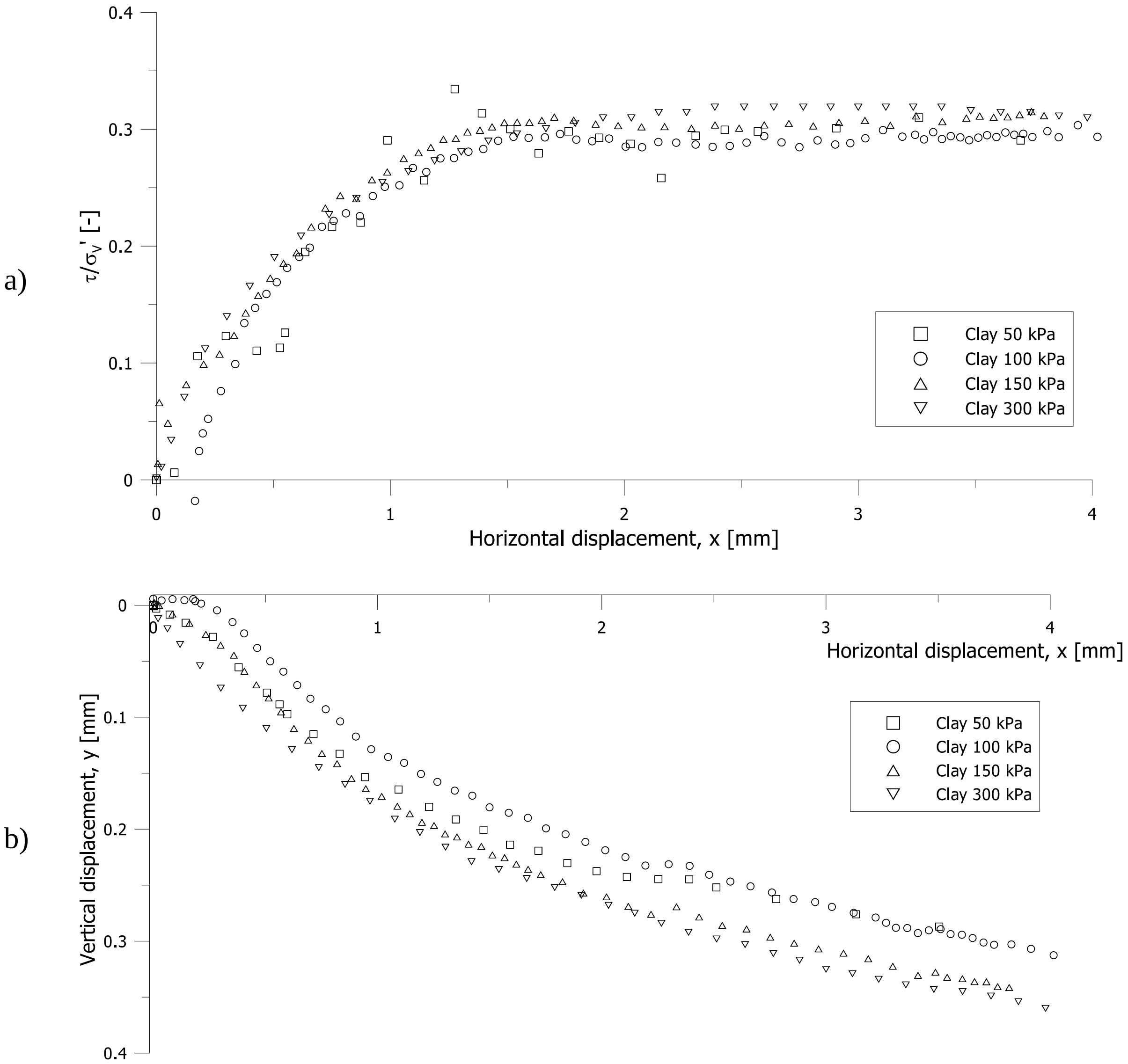

Figure 10. Direct shear tests on Speswhite kaolin samples at different effective vertical

stresses. a) horizontal displacement versus the shear stress/effective vertical stress ratio, b) volumetric change.

Figure 11 shows data from direct shear tests on samples of kaolin clay mixed with CS for values of vertical stress equal to 100, 200 and 300 kPa. All shear tests were conducted under saturated conditions. As reference, the data corresponding to the shear test on kaolin only (already showed in Figure 10) are reported in grey.

Figure 11a shows the horizontal displacement versus t/s'_v. The three samples mixed with CS exhibit a similar behaviour, showing a t/s'_v peak value of about 0.45 and an ultimate value of about 0.37. Moreover, the sample consolidated to 100 kPa shows a slightly higher ultimate t/s'_v than the samples consolidated to 200 and 300 kPa. The samples mixed with CS show a t/s'_v at ultimate conditions about 30% higher than the shear stress/effective vertical stress ratio of samples of kaolin clay only.

Figure 11b shows the horizontal displacement versus the vertical displacement. All the three samples mixed with CS exhibit a compressive behaviour. Vertical compression decreases as the consolidation stress increases. Upon shearing, the CS mixed samples showed to be more compressible than samples prepared with kaolin clay only. Indeed, the vertical deformation of clay-only and clay mixed with CS samples are comparable only for the case of samples consolidated to 300 kPa.

a)

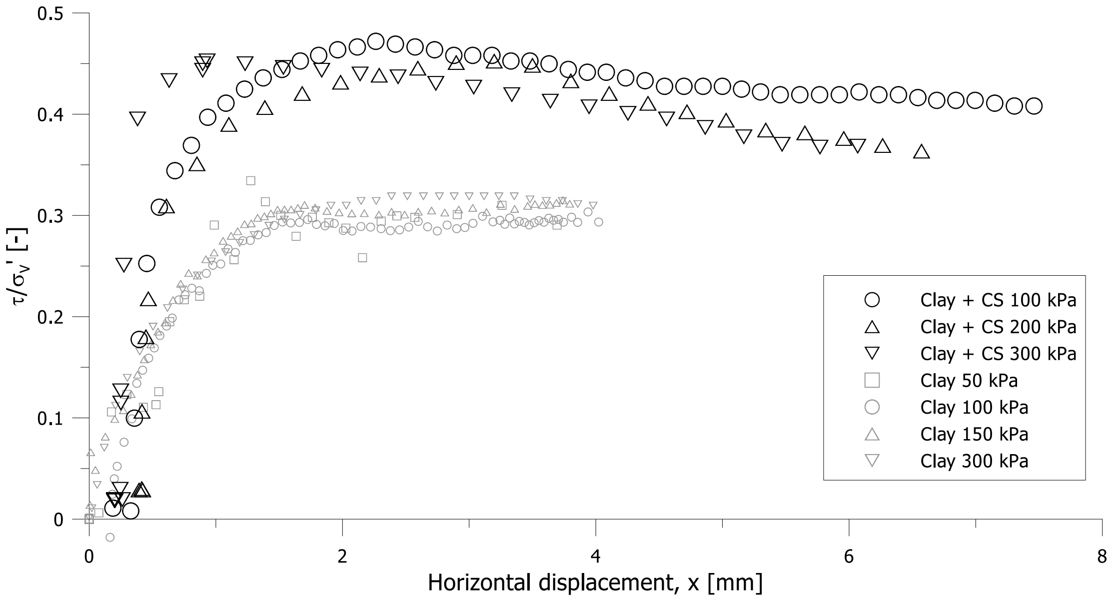
0.5
0.4
0.3
0.2
0.1
0
τ/σv' [-]
0
2
4
6
8
Horizontal displacement, x [mm]
Clay + CS 100 kPa
Clay + CS 200 kPa
Clay + CS 300 kPa
Clay 50 kPa
Clay 100 kPa
Clay 150 kPa
Clay 300 kPa

b)

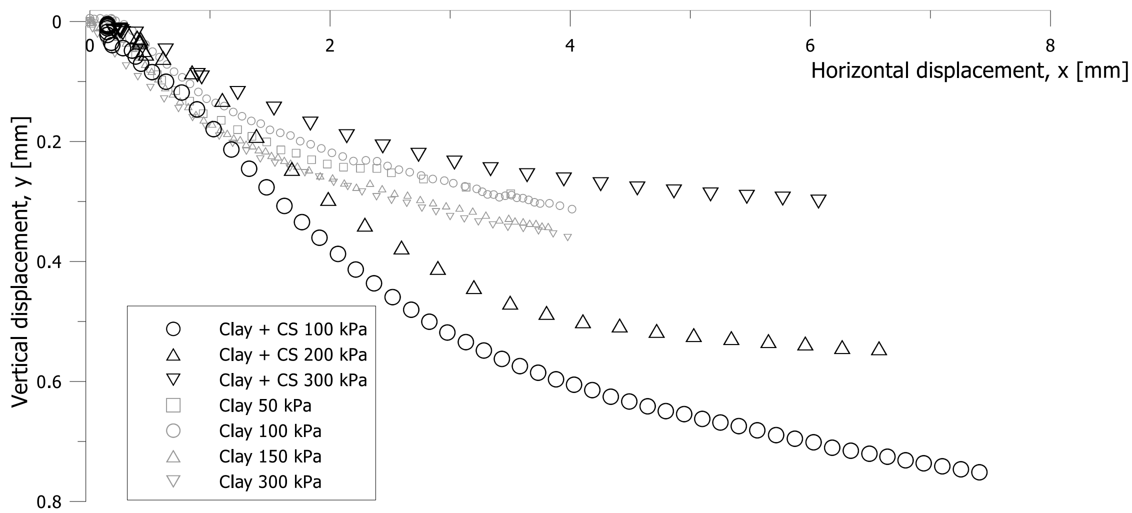
0
0.2
0.4
0.6
0.8
Vertical displacement, y [mm]
0
2
4
6
8
Horizontal displacement, x [mm]
Clay + CS 100 kPa
Clay + CS 200 kPa
Clay + CS 300 kPa
Clay 50 kPa
Clay 100 kPa
Clay 150 kPa
Clay 300 kPa

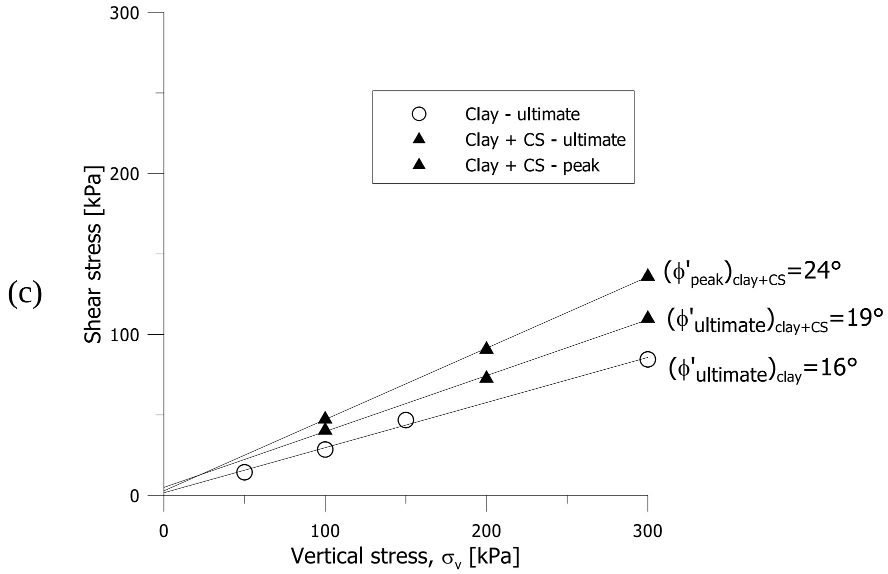

Figure 11 Direct shear test on Speswhite kaolin and CS samples at different vertical stress. a) horizontal displacement versus the shear strss/vertical stress ratio, b) volumetric change and c) peak and ultimate shear envelopes .

In Figure 11 the shear envelope for the ultimate condition of samples of kaolin clay only, and the ultimate conditions and peak conditions for the clay mixed with CS are compared. For peak conditions the clay and CS mixed samples showed a friction angle $\phi'_{peak}=24°$ and a drained cohesion of 3 kPa. For ultimate conditions, these samples showed a friction angle $\phi'_{ultimate}=19°$ and a drained cohesion of 5 kPa.

Mixing with CS increased the friction angle of kaolin clay in terms of both peak and ultimate shear strength. On the other hand, no increase in drained cohesion was recorded, suggesting that no relevant particle bonding due to the addition of CS was created in these samples.

5. MICROSTRUCTURAL INVESTIGATION

A microstructural investigation was carried out on both samples of Leighton Buzzard sand grouted with CS and samples of Speswhite kaolin mixed with CS. Grouted sand was imaged by means of SEM analysis and X-CT scan. SEM analysis was used for imaging and for element analysis samples of clay mixed with CS.

5.1 Sand grouted with CS

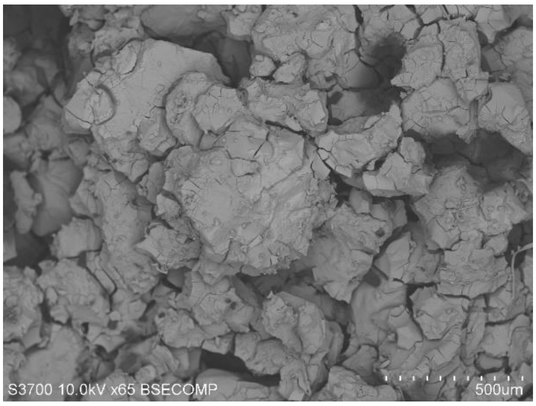

a) magnification factor of 65

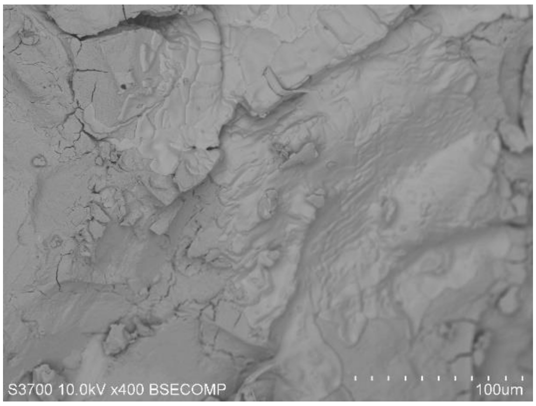

b) magnification factor of 400

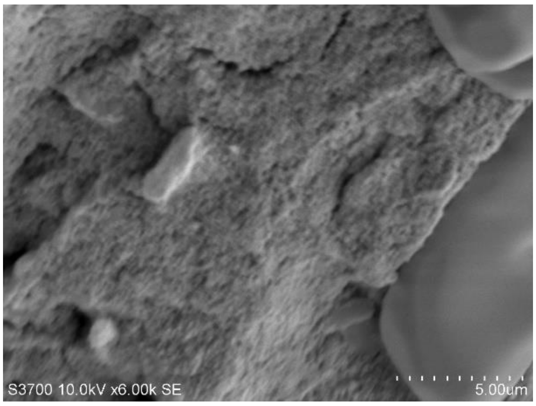

c) magnification factor of 6000

Figure 12. SEM images of Leighton Buzzard sand mixed with CS

Fig 12 shows the SEM image of a sample of Leighton Buzzard sand that was permeated by CS for three different magnification factors at the same location. The sand particles are not visible, they appear to be completely surrounded by a continuous matrix of CS (Figure 12a). The desiccation cracks visible in the CS are due to the oven drying process, which is necessary for imaging in the SEM. At the highest magnification (x6000, Figure 12c), the CS clusters are clearly visible on the surface, and the sand particles are still not visible beneath the coating of colloidal silica, which coats the sand particles in a continuous cover.

In Figure 13 a section of a 3D reconstruction of a sample of sand grouted via permeation with CS is shown. This sample was prepared for shear testing. After curing, but before shearing, the sample was scanned in the X-CT apparatus. No drying was required to be carried out before scanning.

As already demonstrated by the SEM images (Figure 12), CS fills most of the voids present between the sand particles (shown by the dark grey in Figure 13). Air voids would appear black on the image. The whole porosity of the sample now depends only (excluding a few remaining bubbles of air) on the porosity of the CS matrix. The CS matrix itself is not visible as the pore size is at least 2-3 orders of magnitude smaller than the maximum resolution of the scanner (~5 microns for beam settings used). It is evident that no pores remain in the grouted sand sample that are due to the original sand structure.

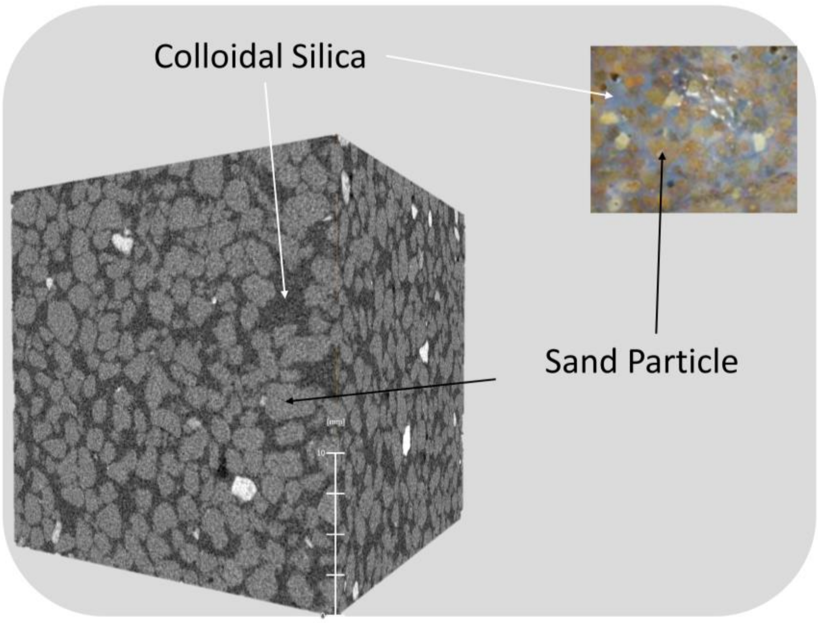

Figure 13. X-CT image of sand grouted with CS

5.2 Clay mixed with CS

Figure 14a shows the SEM image of a sample of kaolin mixed with CS. This sample was consolidated to 1000 kPa and then oven-dried (at 105°C) for at least 24h. The image has a magnification factor of 1000 and the full-scale is approximately 0.1 mm (100 μm). Figure 14a shows a highly heterogeneous pattern of particles of kaolin and a matrix of CS gel. Two distinct areas of the image are highlighted: in the centre (the circle in Figure 14a) it appears that only kaolin particles are present characterised by their hexagonal platy appearance (Mitchell and Soga, 2005) whereas in the surrounding region (e.g. the rectangle in Figure 14a) kaolin particles appear isolated and submerged in the colloidal silica matrix.

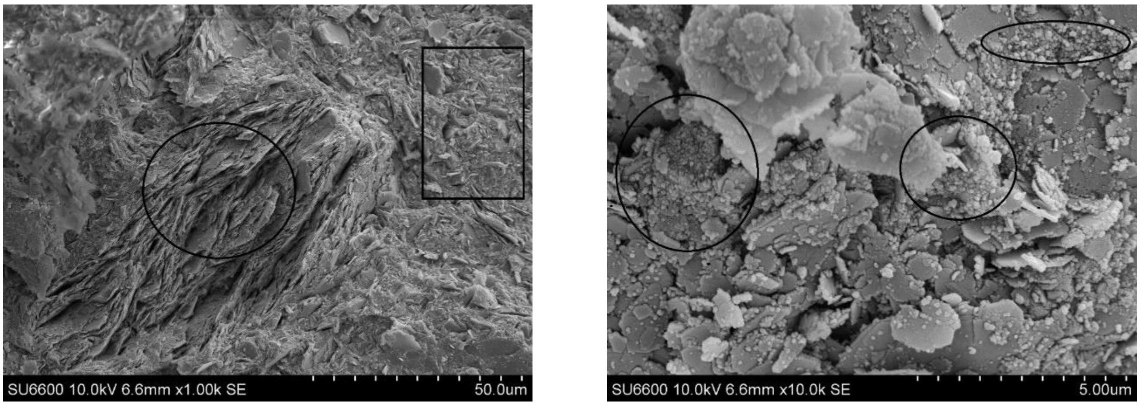

a) Magnification 1k – Energy 10kV. b) Magnification 10k – Energy 10kV.

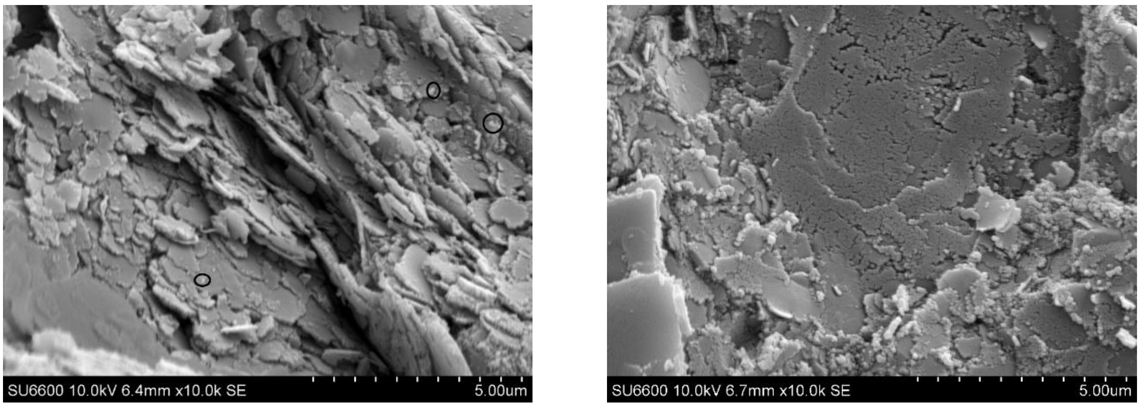

c) Magnification 10k – Energy 10kV.

d) Magnification 10k – Energy 10kV.

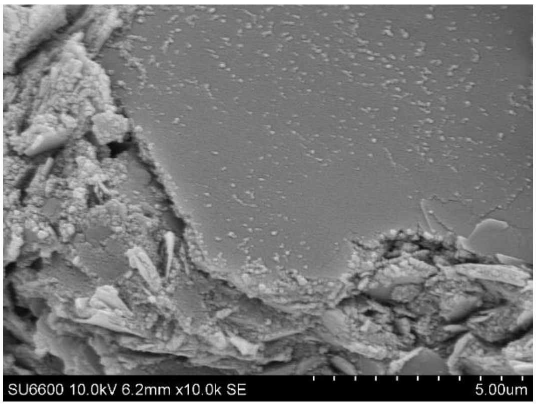

e) Magnification 10k – Energy 10kV.

Figure 14. SEM image on sample of kaolin and CS consolidated to 1000 kPa.

Figure 14b, Figure 14c, Figure 14d and Figure 14e show SEM images from the same sample but with a magnification factor of 10,000 and a full-scale of about 10 μm.

Figure 14b shows a SEM image focused on a region where the kaolin particles prevail. A few clusters of CS particles (highlighted in the Figure) are still visible. Isolated clusters of CS particles can also be identified on kaolin particles as small spheres in the image. It does not appear that the clay particles and the CS matrix create any kind of interconnected configuration.

In the region shown in Figure 14c only kaolin particles are present. Despite the fact that the sample was prepared by mixing kaolin powder with CS, it is clear that the CS particles do not fill the void space present within the structures formed by the kaolin particles, hence, mixing between the CS matrix and the kaolin particles has not occurred at this scale. A few small clusters of CS particles are present in Figure 14c (highlighted by the small circles) however, they are sparse and appear to be negligible in terms of the microstructural configuration.

By contrast, to the clay-rich area, the SEM image in Figure 14d shows a region where CS is mainly present: only CS particles are apparent in the image centre, and no kaolin particles are visibly submerged in the CS matrix. Throughout the whole sample, regions of kaolin particles where CS was poorly present alternated with regions of CS, in which kaolin particles seem to be isolated or not present at all.

Finally, Figure 14e is focused on a very large particle of kaolin, on which particle surface element analysis was carried out in order to investigate whether CS particles coated the clay. Elemental analysis was performed at 5 different points on the clay particle surface and then compared with a similar analysis carried out on a particle of kaolin clay that was not exposed to CS. The average values of the ratio Si/Al for the two different samples are reported in Table 1. For the sample mixed with CS the amount of silica (Si) present on the surface is higher than for the sample of kaolin only. This suggests that, despite not being visible in the SEM images, some CS particles must be present as a coating on the kaolin particle. It is worth noting that similar results were highlighted by Coo et al. (2016) in their study on the effect of nano CuO on kaolin properties.

Table 1. Element analysis on sample of kaolin particles (values are weight [%] ratios).

	Si/Al
Kaolin	1.004
Kaolin + CS	1.725

6. MICROSTRUCTURAL INTERPRETATION OF THE MECHANICAL INTERACTION BETWEEN SOIL AND COLLOIDAL SILICA

6.1 Sand grouted with CS

To support the macroscopic tests with the microstructural information in Figures 12 and

13, a comparison of the conceptual model for particle configuration in sand-only and sand grouted with CS is reported in Figure 15. In the oedometer tests, upon compression, the presence of CS reduced the overall volumetric deformation exhibited by grouted sand samples with increased stiffness over the range of stresses investigated. Considering compression at the microstructural scale, upon vertical compression, particles in ungrouted samples are free to achieve a denser configuration by rearranging into the pore space. By comparison, the rearrangement of sand particles in the grouted samples is inhibited by the presence of the colloidal silica, which occupies any accessible pore space around the sand particles. Hence, the presence of CS in the pore space, not only generates a denser sample but also a stiffer one, in agreement with the macroscopic tests.

Considering the microscopic scale, increased peak shear strength occurs because the continuous matrix of CS that surrounds the sand particles provides a weak bonding between particles, which macroscopically generates some cohesion until the CS matrix is broken along the shear plane. After failure, the presence of the CS prevents compression upon shearing, forcing a dilative behaviour (Figure 7), which in turn increases the peak resistance. However, once the strength of the CS matrix is overwhelmed the sand particle-to-particle friction controls the ultimate conditions.

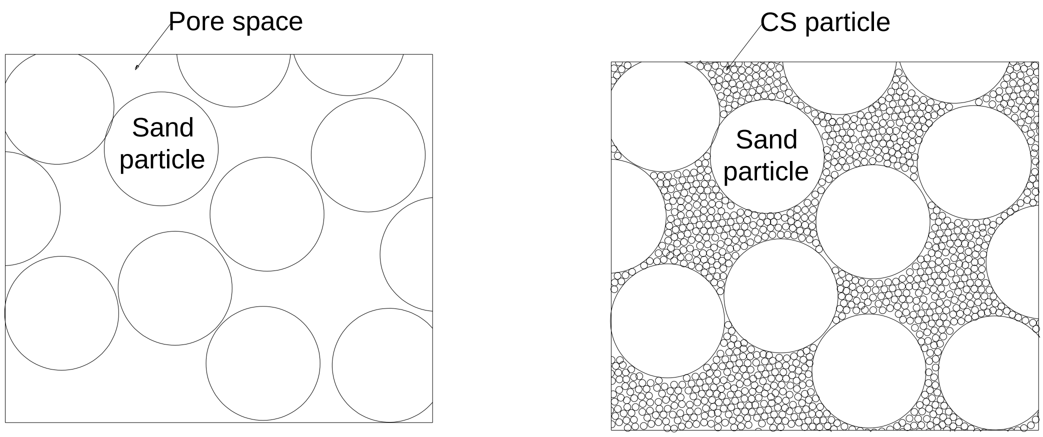

a) b)

Figure 15. Conceptual model for particle configuration in sand grouted with CS. a) Not grouted sand and b) grouted sand

6.2 Clay mixed with CS

To understand how the microstructural information can inform the results of the macroscopic tests, a simplified sketch is shown of an ungrouted clay (Figure 16a) and of the two different characteristic regions identifiable in the SEM image: sub-regions where kaolin particles dominate (Figure 16b) and sub-regions where a matrix of CS particles dominates (Figure 16c). In the macroscopic test, upon vertical compression, the clay samples mixed with CS showed reduced volumetric deformation, with increased stiffness only at low stresses, and above 100kPa the compressibility of the clay-CS samples became similar to that of the clay only samples. In the sub-regions where kaolin particles dominate (Figure 16b) the clay particle configuration is similar to the arrangement in clay-only samples, however, since the pore water is shared with the sub-regions where CS dominates, the clay particle structure is denser and therefore stiffer. Similarly, in the CS sub-regions (Figure 16c) the density is higher than a sample with colloidal silica particles only, again because of the reduced amount of water, as water is shared with the sub-regions of clay particles. Both sub-regions are therefore expected to be at higher density and consequently exhibit a stiffer behaviour. Upon vertical compression, as the vertical stress increases (exceeding 100 kPa) the difference in density (and water content) between the clay-CS and the clay-only samples decreases, until the compressibility of both become similar (Figure 9a). Such behaviour suggests that between the two sub-regions, the regions dominated by the clay particles are controlling the macroscopic compressive behaviour.

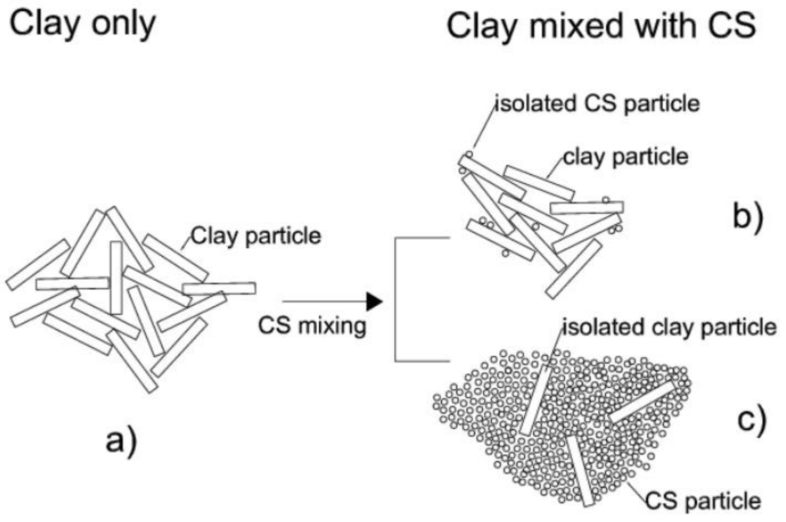

Figure 16. Particle configuration for kaolin mixed with CS samples. a) clay only , b) clay mixed with CS where kaolin particles dominate and c) clay mixed with CS where CS particles dominate

The micro-mechanisms controlling the shear strength of clays are not well understood, and are therefore difficult to discuss here (Morgenstern and Tchalenko, 1967, Sridharan and Venkatappa Rao, 1973, Burland, 1990, Tarantino and Tombolato, 2005). At a macroscopic scale, the mixing of CS increased the peak and ultimate shear strength of the clay mixture but did not have any effect on the drained cohesion. One may speculate that, in terms of shear strength, the presence of sub-regions of CS at high density hampers the formation of a shear surface, resulting in an increase in the energy required for failure (i.e. increasing the peak shear stress). Furthermore, the silica to silica contacts would be expected to have higher frictional resistance than the kaolin to kaolin contacts (Morrow et al., 2000) which explains why the ultimate conditions of the clay-CS mixtures remain higher than the clay only samples (in contrast to the grouted sands). Finally as suggested by the SEM pictures (Figure 14), CS does not provide any bonding between clay particles and therefore no increase in cohesion should be expected.

9. CONCLUSIONS

This paper has presented the drained stress-strain behaviour of CS gel, sands grouted with CS and clay mixed with CS. Observations of the microstructural properties of the CS grouted sand and clays have enabled the development of conceptual material models that can explain the macroscopic observations.

For CS grouted sands:

- the presence of CS reduces the overall volumetric deformation during compression and increases the stiffness, when compared with sand-only. This occurs because the colloidal silica gel occupies all the accessible pore space, thus inhibiting the rearrangement of particles upon compaction. This generates a sample that is both denser and stiffer.
- the presence of CS reduces the overall volumetric deformation and enhances the peak shear strength. This occurs because CS provides a weak bonding between sand particles, generating cohesion. Once this matrix is broken, the presence of CS in the pore space forces a dilative behaviour increasing the peak resistance. After failure of the CS bonds, the sand particle-to-particle friction controls the ultimate conditions.

For CS clay mixtures:

- The presence of CS reduces the volumetric deformation and increases the stiffness for low values of stress (~100kPa). This occurs because the CS grouted clay maintains distinct sub-regions of kaolin and of CS, these sub-regions compete for pore water resulting in a denser and stiffer material. This difference in water content decreases as compression increases and water is expelled.
- The presence of CS increases both the peak and the ultimate shear strength but does not effect the drained cohesion. This may occur because the sub-regions of CS impede the formation of a shear surface, thus increasing the peak shear stress, and the silica to silica contacts have a higher frictional resistance than the kaolin to kaolin contacts increasing the ultimate shear-strength. Finally, since the CS is not incorporated into the bonds between clay particles, no increase in cohesion is observed.

CS is well known for its low hydraulic conductivity and application for controlling fluid flow in porous media. Its undrained behaviour has been previously reported suggesting its application for short-term stability problems. This paper illustrates for the first time that even under drained conditions CS can provide mechanical improvement; for grouted sands increasing further the stiffness beyond that of sands and enhancing the peak friction angle. Thus while still having a very low hydraulic conductivity (~10^{-10} m/s), typical of intact clay. This paper also presents results on clays mixed with CS which have the potential to be novel materials. Their application could be deployed in environments where not only hydraulic containment is critical but where reduced deformation and enhanced resistance to shearing would be beneficial, for example in landfill capping or in the outer fill layers of embankments designed to minimise internal seepage and infiltration.

ACKNOWLEDGEMENTS

The authors gratefully acknowledge the financial support of the Research Councils' UK Energy Programme under grant EP/L014041/1, "Decommissioning, Immobilisation and Storage Solutions for Nuclear Waste Inventories (DISTINCTIVE).

REFERENCES

AXELSSON, M. 2006. Mechanical tests on a new non-cementitious grout, silica sol: A laboratory study of the material characteristics. *Tunnelling and underground space technology,* 21, 554-560.

BAHADUR, A., HOLTER, K. & PENGELLY, A. Cost-effective pre-injection with rapid hardening microcement and colloidal silica for water ingress reduction and stabilisation of adverse conditions in a headrace tunnel. Underground Space–The 4th Dimension of Metropolises, Three Volume Set+ CD-ROM: Proceedings of the World Tunnel Congress 2007 and 33rd ITA/AITES Annual General Assembly, Prague, May 2007, 2007. CRC Press, 297.

BSI 1990. BS1377-7:1990. *Methods of Test for Soils for Civil Engineering Purposes: Shear strength tests (total stress).* London: BSI: British Standards Institution.

BURLAND, J. 1990. On the compressibility and shear strength of natural clays. *Geotechnique,* 40, 329-378.

BUTRÓN, C., AXELSSON, M. & GUSTAFSON, G. 2009. Silica sol for rock grouting: Laboratory testing of strength, fracture behaviour and hydraulic conductivity. *Tunnelling and underground space technology,* 24, 603-607.

BUTRÓN, C., GUSTAFSON, G., FRANSSON, Å. & FUNEHAG, J. 2010. Drip sealing of tunnels in hard rock: A new concept for the design and evaluation of permeation grouting. *Tunnelling and underground space technology,* 25, 114-121.

CHANGIZI, F. & HADDAD, A. 2017. Improving the geotechnical properties of soft clay with nano-silica particles. *Proceedings of the Institution of Civil Engineers-Ground Improvement,* 170, 62-71.

COO, J. L., SO, Z. P. & NG, C. W. 2016. Effect of nanoparticles on the shrinkage properties of clay. *Engineering Geology,* 213, 84-88.

FUNEHAG, J. & FRANSSON, Å. 2006. Sealing narrow fractures with a Newtonian fluid: Model prediction for grouting verified by field study. *Tunnelling and underground space technology,* 21, 492-498.

FUNEHAG, J. & GUSTAFSON, G. 2008. Design of grouting with silica sol in hard rock–New design criteria tested in the field, Part II. *Tunnelling and underground space technology,* 23, 9-17.

GALLAGHER, P. M., CONLEE, C. T. & ROLLINS, K. M. 2007. Full-scale field testing of colloidal silica grouting for mitigation of liquefaction risk. *Journal of Geotechnical and Geoenvironmental Engineering,* 133, 186-196.

GALLAGHER, P. M. & FINSTERLE, S. 2004. Physical and numerical model of colloidal silica injection for passive site stabilization. *Vadose Zone Journal,* 3, 917-925.

GALLAGHER, P. M. & LIN, Y. 2009. Colloidal silica transport through liquefiable porous media. *Journal of geotechnical and geoenvironmental engineering,* 135, 1702-1712.

GALLAGHER, P. M. & MITCHELL, J. K. 2002. Influence of colloidal silica grout on liquefaction potential and cyclic undrained behavior of loose sand. *Soil Dynamics and Earthquake Engineering,* 22, 1017-1026.

GALVANI, A. 2003. *Resistenza a taglio di un argilla non satura ricostituita in laboratorio.* M.Eng., University of Trento.

HAKEM, N., AL MAHAMID, I., APPS, J. & MORIDIS, G. Sorption of cesium and strontium on Savannah River soils impregnated with colloidal silica. International Containment Technology Conference, 1997. Petersburg:[sn], 652-657.

HAZEN, A. 1893. Some physical properties of sand and gravels. Massachusetts State Board of Health. *24th Annual Report*.

HUANG, Y. & WANG, L. 2016. Laboratory investigation of liquefaction mitigation in silty sand using nanoparticles. *Engineering Geology,* 204**,** 23-32.

ILER, R. K. 1979. *The Chemistry of Silica: Solublity, Polymerization, Colloid and Surface Properties, and Biochemistry,* John Wiley & Sons.

IRANPOUR, B. 2016. The influence of nanomaterials on collapsible soil treatment. *Engineering Geology,* 205**,** 40-53.

JURINAK, J. & SUMMERS, L. 1991. Oilfield applications of colloidal silica gel. *SPE production engineering,* 6**,** 406-412.

LIAO, H., HUANG, C. & CHAO, B. 2003. Liquefaction resistance of a colloid silica grouted sand. *Grouting and ground treatment.*

MANCHESTER, K., ZALUSKI, M., NORTH-ABBOTT, M., TRUDNOWSKI, J., BICKFORD, J. & WRAITH, J. Grout selection and characterization in support of the colloidal silica barrier deployment at Brookhaven National Laboratory. Proc. 2001 International Contain. and Remed. Technol. Conf. and Exhib., 10-13 June, 2001. Orlando, FL, 2001.

MITCHELL, J. & SOGA, K. 2005. Fundamentals of Soil Behavior, Jon Wiley and Sons Inc. *Hoboken, NJ*.

MOLLAMAHMUTOGLU, M. & YILMAZ, Y. 2010. Pre-and post-cyclic loading strength of silica-grouted sand. *Proceedings of the Institution of Civil Engineers-Geotechnical Engineering,* 163**,** 343-348.

MORGENSTERN, N. & TCHALENKO, J. 1967. Microscopic structures in kaolin subjected to direct shear.

MORIDIS, G., APPS, J., PERSOFF, P., MYER, L., MULLER, S., PRUESS, K. & YEN, P. A field test of a waste containment technology using a new generation of injectable barrier liquids. 1996a. Medium: ED; Size: 16 p.

MORIDIS, G., JAMES, A. & OLDENBURG, C. 1996b. Development of a design package for a viscous barrier at the Savannah River site. Lawrence Berkeley National Lab., CA (United States). Funding organisation: USDOE Office of Environmental Restoration and Waste Management, Washington, DC (United States).

MORIDIS, G., PERSOFF, P., APPS, J., MYER, L., PRUESS, K. & YEN, P. 1995. A field test of permeation grouting in heterogeneous soils using a new generation of barrier liquids. *Committed To Results: Barriers for Long-Term Isolation. ER,* 95.

MORIDIS, G. J., FINSTERLE, S. & HEISER, J. 1999. Evaluation of alternative designs for an injectable barrier at the Brookhaven National Laboratory Site, Long Island, New York. *Water Resources Research,* 35**,** 2937-2953.

PEDROTTI, M., WONG, C., EL MOUNTASSIR, G. & LUNN, R. 2017. An analytical model for the control of silica grout penetration in natural groundwater systems. *Tunnelling and Underground Space Technology,* 70**,** Pages 105-113.

PEDROTTI, M. T., A. 2018. Effective stresses for unsaturated states stemming from an experimental investigation into the microstructure of unsaturated clay. *Geomechanics for Energy and Environment*.

PERSOFF, P., APPS, J., MORIDIS, G. & WHANG, J. M. 1999. Effect of dilution and contaminants on sand grouted with colloidal silica. *Journal of geotechnical and geoenvironmental engineering,* 125**,** 461-469.

PERSOFF, P., FINSTERLE, S., MORIDIS, G. J., APPS, J., PRUESS, K. & MULLER, S. J. 1995. Injectable barriers for waste isolation. Lawrence Berkeley Lab., CA (United States).

SKEMPTON, A. W. & JONES, O. 1944. Notes on the compressibility of clays. *Quarterly Journal of the Geological Society,* 100, 119-135.

SRIDHARAN, A. & NAGARAJ, H. 2000. Compressibility behaviour of remoulded, fine-grained soils and correlation with index properties. *Canadian Geotechnical Journal,* 37, 712-722.

SRIDHARAN, A. & VENKATAPPA RAO, G. 1973. Mechanisms controlling volume change of saturated clays and the role of the effective stress concept. *Geotechnique,* 23, 359-382.

TARANTINO, A. & TOMBOLATO, S. 2005. Coupling of hydraulic and mechanical behaviour in unsaturated compacted clay. *Geotechnique,* 55, 307-317.

TAYLOR, D. 1948. *Fundamentals of soil mechanics*, Chapman And Hall, Limited.; New York.

YATES, P. C. Kinetic of gel formation of colloidal silica sols. 200th National meeting: Abstract, 1990.